An analytical study of two-dimensional buckling of thin films on compliant substrates

J. Song
Department of Mechanical Science and Engineering, University of Illinois at Urbana-Champaign, Urbana, Illinois 61801, USA

H. Jiang
Department of Mechanical and Aerospace Engineering, Arizona State University, Tempe, Arizona 85287, USA

W. M. Choi and D. Y. Khang
Department of Materials Science and Engineering, Beckman Institute, and Seitz Materials Research Laboratory, University of Illinois at Urbana-Champaign, Urbana, Illinois 61801, USA

Y. Huang[a)]
Department of Civil and Environmental Engineering and Department of Mechanical Engineering, Northwestern University, Evanston, Illinois 60208, USA

J. A. Rogers
Department of Materials Science and Engineering, Beckman Institute, University of Illinois at Urbana-Champaign, Urbana, Illinois 61801, USA and Seitz Materials Research Laboratory, University of Illinois at Urbana-Champaign, Urbana, Illinois 61801, USA

(Received 31 July 2007; accepted 30 October 2007; published online 3 January 2008)

A stiff thin film on a heated compliant substrate may buckle when the system is cooled due to the thermal expansion mismatch between the film and substrate. Highly ordered and disordered herringbone patterns (wavy structures) then emerge as the system continues to cool. We have established an analytic approach to study one-dimensional, checkerboard, and ordered herringbone buckling patterns. The analytical approach gives the buckle wave length and amplitude in terms of the thin film and substrate elastic properties, thin film thickness, and the thermal strain. It is shown that the herringbone mode has the lowest energy, which explains why this mode is frequently observed in experiments. These classes of materials might be interesting as a route to high performance electronics with full, two-dimensional stretchability. © *2008 American Institute of Physics*. [DOI: 10.1063/1.2828050]

I. INTRODUCTION

Nonlinear buckling of a stiff thin film on a compliant substrate can be useful in stretchable electronics, which has many important applications, including eyelike digital cameras,[1] comformable skin sensors,[2] intelligent surgical gloves,[3] and structural health monitoring devices.[4] Recent demonstrations[5–7] involved the use of buckled, one-dimensional (1D) "wavy" geometries in nanoribbons (thickness between tens and hundreds of nanometers and widths in micron range) of silicon and gallium arsenide to achieve uniaxial stretchability in metal oxide semiconductor field effect transistors, metal semiconductor field effect transistors, *p-n* junction diodes, and Schottky diodes.

Choi *et al.*[8] produced biaxially stretchable wavy silicon nanomembranes on elastomeric poly(dimethylsiloxane) (PDMS) substrate to provide full two-dimensional (2D) stretchability. As illustrated in Fig. 1, the approach involved first the delineation of nanomembranes of Si (thickness between 55 and 320 nm) from silicon-on-insulator (SOI) wafers [top silicon is (100)] by photolithographic processing and etching of the top silicon. Next, the buried SiO_2 layer is removed by hydrofluoric acid to yield membranes that rest on, but are not bonded to, the underlying wafer. The lateral dimensions of these membranes are typically a few millimeters by a few millimeters. Casting and curing prepolymers of PDMS against polished silicon wafers generated flat, elastomeric substrates (about 4 mm thick). Heating the substrates in a convection oven induced a controlled degree of isotropic thermal expansion. Contacting the prestrained PDMS to the Si nanomembranes formed strong chemical bonds between these materials. Peeling back the PDMS and flipping it over yielded Si/PDMS structures [Fig. 1(a)]. Cooling to room temperature released the thermally induced prestrain, thereby causing the PDMS to relax back to its unstrained state [Fig. 1(b)]. This relaxation led to the spontaneous formation of 2D wavy patterns on the surface. These patterns exhibited different behaviors near the edges, where 1D periodic waves [shown schematically in Fig. 2(a)] predominated, at inner regions, where 2D herringbone layouts [shown schematically in Figs. 1(c) and 2(c)] were typically observed, and near the centers, where disordered herringbone structures often occurred.

Figures 3(a)–3(c) show, respectively, the optical, atomic force microscope, and scanning electron microscope images

[a)]Author to whom correspondence should be addressed. Tel.: +1-847-242-9146. FAX: +1-847-491-4011.
Electronic mail: y-huang@northwestern.edu.

 © 2008 American Institute of Physics

Downloaded 03 Jan 2008 to 129.105.86.133. Redistribution subject to AIP license or copyright; see http://jap.aip.org/jap/copyright.jsp

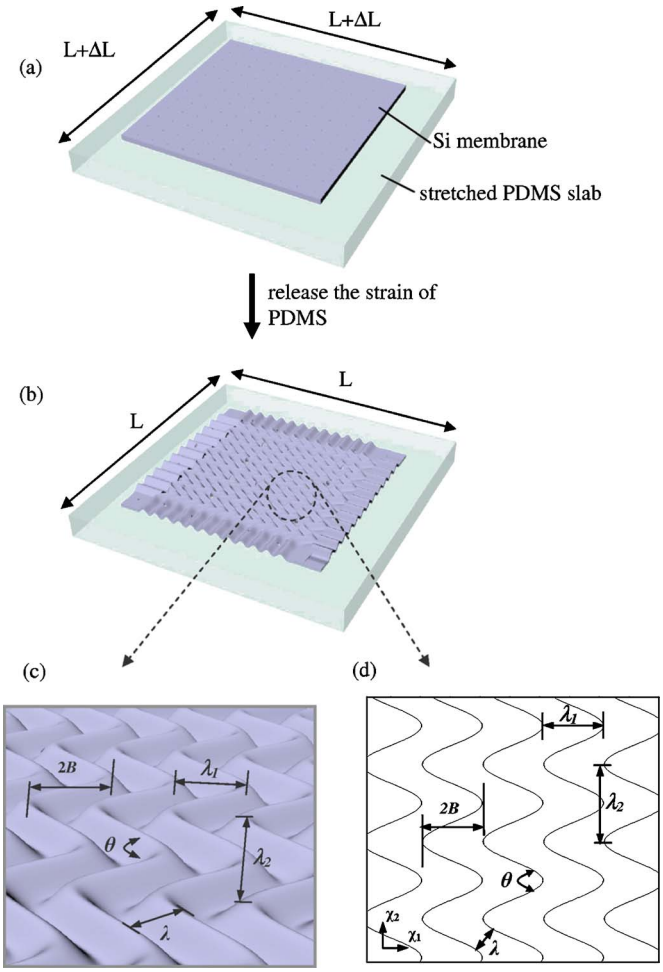

FIG. 1. (Color online) Schematic illustration of the process for fabricating two-dimensional wavy Si nanomembranes on a PDMS substrate: (a) Si membrane is bonded on the stretched PDMS; (b) formation of 2D wavy patterns when PDMS is relaxed; (c) Herringbone mode; and (d) top-down view of the herringbone mode. The parameters are illustrated in (c) and (d), including the short wavelength λ, long wavelength λ_2, and jogs wavelength λ_1, the amplitude B of the jogs in the plane of the film, and the jog angle θ.

of herringbone waves for the case of a silicon film of 100 nm thickness (the lateral dimension is 4×4 mm^2) on a PDMS substrate. The PDMS substrate was first heated in a convection oven to 150 °C. Contacting the heated PDMS to the processed SOI wafer and then peeling it off again transferred the entire nanomembrane to the PDMS. Continued heating in the convection oven for a few minutes facilitated the formation of strong adhesive bonds between the membrane and the PDMS. The nanomembrane/PDMS structure was cooled to room temperature (25 °C) to release the thermally induced

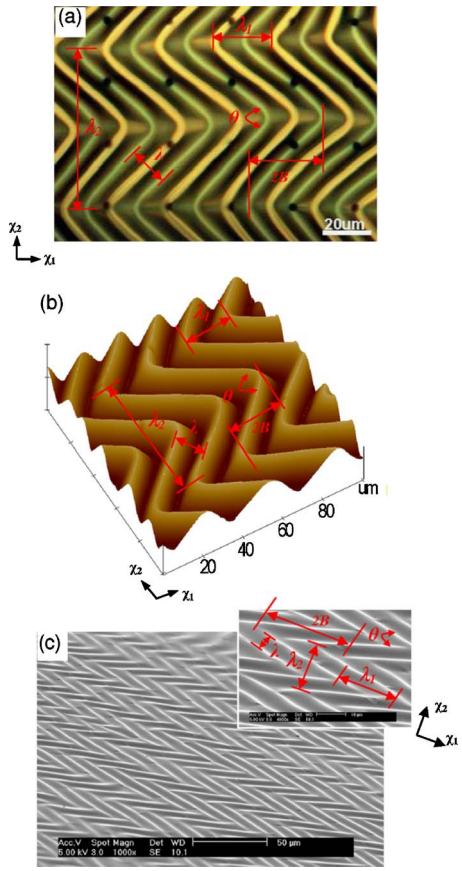

FIG. 3. (Color online) (a) Optical, (b) atomic force, and (c) scanning electron micrographs of a 2D wavy Si nanomembrane on PDMS. The thickness of the silicon is 100 nm. These images highlight the highly periodic nature of the wavy patterns. The parameters involved are the short wavelength λ, long wavelength λ_2, and jogs wavelength λ_1, the amplitude B of the jogs in the plane of the film, and the jog angle θ.

strain. The images in Fig. 3 clearly show that the herringbone patterns are characterized by zigzag structures that define two characteristic directions, even though the compressive strain is completely isotropic. The herringbone region is characterized by the perpendicular distance between adjacent sinusoidal contours, which we refer as the short wavelength λ, the amplitude of wave out of the plane of the film A, and a longer distance $\lambda_2=2\pi/k_2$ associated with the separation between adjacent jogs in the herringbone structure, which we refer to as the long wavelength. Other characteristic lengths are the jogs wavelength $\lambda_1=2\pi/k_1$, the amplitude B of the jogs in the plane of the film, and the jog angle θ. Except for the amplitude A, all parameters are illustrated in Figs. 3(a)–3(c), as well as in Figs. 1(c) and 1(d) where λ_2 and λ_1

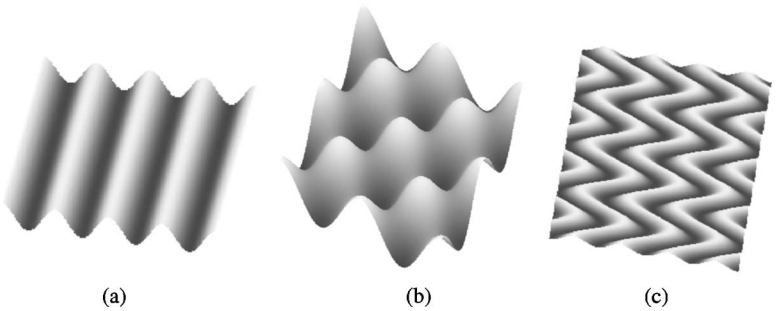

FIG. 2. Schematic illustrations of different buckling modes: (a) 1D mode, (b) checkerboard mode from Eq. (11), and (c) herringbone mode from Eq. (25) with $A=1.0$ μm, $k_1=0.309$ μm^{-1}, $B=10$ μm, and $k_2=0.139$ μm^{-1}.

Downloaded 03 Jan 2008 to 129.105.86.133. Redistribution subject to AIP license or copyright; see http://jap.aip.org/jap/copyright.jsp

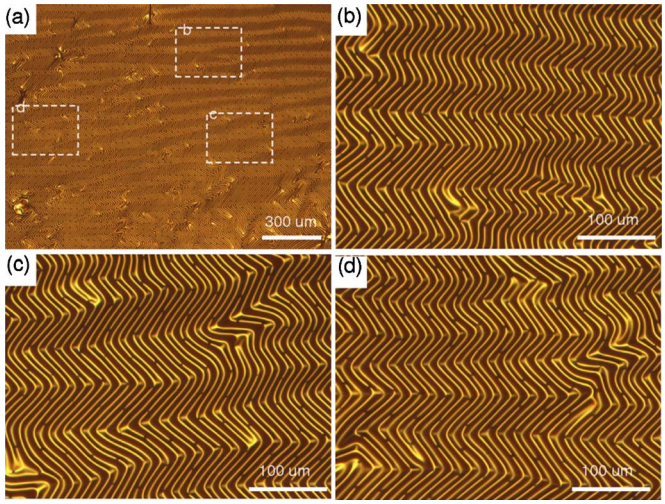

FIG. 4. (Color online) (a) Optical micrographs of a 2D wavy Si nanomembrane on PDMS and its different locations [(b)–(d)]. The thickness of the silicon is 100 nm. These images highlight the large variation of long wavelength in the same sample.

are along the x_2 and x_1 directions, respectively. Further illustrations will be provided after Eq. (25). The short wavelength is 12.6 (±0.37) μm and the amplitude is 0.64 (±0.07) μm for Figs. 3(a)–3(c). The jog angle θ is about 90° over a large area. By contrast, the long wavelength associated with the herringbone layout exhibits a broad range of values from 40 to 120 μm. Figure 4 shows the herringbone pattern at various locations in a sample. A large variation of the long wavelength is clearly observed.

There are extensive numerical but not analytical studies on the buckling of two-dimensional stiff thin films on compliant substrates. Chen and Hutchinson[9,10] used the finite element method to study the dependence of energy in the buckled state on the parameters of the geometry of herringbone mode. They obtained the herringbone structures and showed that the energy is insensitive to the long wavelength and the jog angle is about 90°. Huang *et al.*[11,12] developed a spectral method to study the 2D buckling problem, and identified different buckling modes such as the checkerboard in Fig. 2(b) and the herringbone mode in Fig. 2(c). These two modes occur when the prestrain just exceeds the critical buckling strain and when the prestrain becomes large, respectively. Disordered herringbone mode occurs as the prestrain continues to increase. Huang and Suo[13] used the finite difference method to reveal rich dynamics of elastic film/viscous layer with many unstable equilibrium configurations for 1D wrinkling. Peterson *et al.*[14] compared 1D and 2D buckling modes in thin silicon-germanium films on borophosphorosilicate glass substrate experimentally and found that 1D buckling mode exhibits slower buckling and lower final steady state buckling amplitude. Huang and Im[15] used the spectral method to study the two-dimensional wrinkling of a stiff thin film on a viscoelastic substrate. The herringbone structures represent a minimum elastic energy configuration that reduces the overall in-plane stress in the system and relieves biaxial compression in both directions, and are therefore preferred over large areas, compared to the 1D [Fig. 2(a)] and checkerboard modes [Fig. 2(b)].

The objective of this paper is to perform an analytical study of these different buckling modes including 1D, checkerboard, and herringbone. The analytical study gives the wavelength and amplitude directly in terms of the film and substrate elastic properties, the thin film thickness, and the prestrain. They have the advantage over the numerical methods to isolate each buckling mode and calculate its energy. The energies for different buckling modes are compared, which explains why the herringbone mode is often observed in experiments. The paper is outlined as follows. The method of energy minimization for buckling analysis is described in Sec. II. The analytical solution for the checkerboard mode is obtained in Sec. III. The herringbone and 1D modes are studied in Secs. IV and V, respectively. The results are presented in Sec. VI.

II. BUCKLING ANALYSIS

A. The thin film

The thin film is subjected to compressive uniform biaxial membrane strains, ε_{11}^0 and ε_{22}^0, and buckles once ε_{11}^0 and ε_{22}^0 exceed a critical value. The thin film is modeled as an elastic Von Karman plate with finite rotation.[16] The membrane strain $\varepsilon_{\alpha\beta}$ is related to the in-plane displacements $u_1\ (x_1,x_2)$ and $u_2\ (x_1,x_2)$ and out-of-plane displacement $w(x_1,x_2)$ by

$$\varepsilon_{\alpha\beta}=\varepsilon_{\alpha\beta}^0+\frac{1}{2}\left(\frac{\partial u_\alpha}{\partial x_\beta}+\frac{\partial u_\beta}{\partial x_\alpha}\right)+\frac{1}{2}\frac{\partial w}{\partial x_\alpha}\frac{\partial w}{\partial x_\beta}, \tag{1}$$

where $\alpha,\beta=1,2$.

The Hooke law gives the membrane forces in the thin film,

$$N_{\alpha\beta}=h_f\bar{E}_f[(1-\nu_f)\varepsilon_{\alpha\beta}+\nu_f(\varepsilon_{11}+\varepsilon_{22})\delta_{\alpha\beta}], \tag{2}$$

where $\alpha,\beta=1,2$, h_f is the film thickness, and $\bar{E}_f=E_f/(1-\nu_f^2)$ and ν_f are the plane-strain modulus and Poisson's ratio, respectively. The force equilibrium gives the shear and normal tractions at the film/substrate interface as

$$T_\alpha=\frac{\partial N_{\alpha1}}{\partial x_1}+\frac{\partial N_{\alpha2}}{\partial x_2}, \tag{3}$$

where $\alpha=1,2$ and

$$T_3=-\frac{h_f^3\bar{E}_f}{12}\left(\frac{\partial^4 w}{\partial x_1^4}+2\frac{\partial^4 w}{\partial x_1^2\partial x_2^2}+\frac{\partial^4 w}{\partial x_2^4}\right)+\frac{\partial}{\partial x_1}\left(N_{11}\frac{\partial w}{\partial x_1}+N_{21}\frac{\partial w}{\partial x_2}\right)+\frac{\partial}{\partial x_2}\left(N_{12}\frac{\partial w}{\partial x_1}+N_{22}\frac{\partial w}{\partial x_2}\right). \tag{4}$$

The strain energy density in the thin film consists of the bending energy density W_b and membrane energy density W_m given by

Downloaded 03 Jan 2008 to 129.105.86.133. Redistribution subject to AIP license or copyright; see http://jap.aip.org/jap/copyright.jsp

$$W_b = \frac{\bar{E}_f h_f^3}{24}\left[\left(\frac{\partial^2 w}{\partial x_1^2}\right)^2 + \left(\frac{\partial^2 w}{\partial x_2^2}\right)^2 + 2\nu_f \frac{\partial^2 w}{\partial x_1^2}\frac{\partial^2 w}{\partial x_2^2} + 2(1-\nu_f) \times \left(\frac{\partial^2 w}{\partial x_1 \partial x_2}\right)^2\right] \quad (5)$$

and

$$W_m = \tfrac{1}{2}(N_{11}\varepsilon_{11} + N_{12}\varepsilon_{12} + N_{21}\varepsilon_{21} + N_{22}\varepsilon_{22}). \quad (6)$$

B. The substrate

The substrate is modeled as a semi-infinite three-dimensional elastic solid.[17] The displacements u_i (x_1, x_2, x_3) $(i=1,2,3)$ in the substrate satisfy the displacement continuity with u_α and w in the thin film across the film/substrate interface. The strains ε_{ij} in the substrate are given by

$$\varepsilon_{ij} = \frac{1}{2}\left(\frac{\partial u_i}{\partial x_j} + \frac{\partial u_j}{\partial x_i}\right), \quad (7)$$

where the substrates $i,j=1,2,3$. The Hooke law gives the stress as

$$\sigma_{ij} = \frac{E_s}{1+\nu_s}\varepsilon_{ij} + \frac{\nu_s E_s}{(1+\nu_s)(1-2\nu_s)}(\varepsilon_{11}+\varepsilon_{22}+\varepsilon_{33})\delta_{ij}, \quad (8)$$

where the substrates $i,j=1,2,3$. The equilibrium equation is

$$\frac{\partial \sigma_{i1}}{\partial x_1} + \frac{\partial \sigma_{i2}}{\partial x_2} + \frac{\partial \sigma_{i3}}{\partial x_3} = 0 \quad (9)$$

where $i=1,2,3$. The tractions at the film/substrate interface satisfy the continuity with T_α in Eq. (3) and T_3 in Eq. (4).

The strain energy density in the substrate is given by

$$W_s = \tfrac{1}{2}(\sigma_{11}\varepsilon_{11} + \sigma_{12}\varepsilon_{12} + \sigma_{13}\varepsilon_{13} + \sigma_{21}\varepsilon_{21} + \sigma_{22}\varepsilon_{22} + \sigma_{23}\varepsilon_{23} + \sigma_{31}\varepsilon_{31} + \sigma_{32}\varepsilon_{32} + \sigma_{33}\varepsilon_{33}). \quad (10)$$

C. The total energy

The total energy U_{total} consists of three parts: the bending energy U_b and membrane energy U_m in the thin film, and the strain energy U_s in the substrate, which can be obtained from the integration of the corresponding energy densities W_b, W_m, and W_s in Eqs. (5), (6), and (10), respectively. The minimization of the total energy with respect to the wavelength and amplitude then gives different buckling modes, such as the checkerboard in Sec. III, herringbone in Sec. IV, and 1D in Sec. V.

III. CHECKERBOARD BUCKLING MODE

The out-of-plane displacement of generalized checkerboard mode, as shown in Fig. 2(b), is given by

$$w = A\cos(k_1 x_1)\cos(k_2 x_2), \quad (11)$$

where the amplitude A and the wave numbers k_1 and k_2 along the x_1 and x_2 directions are to be determined. The checkerboard mode is the mode for $k_1=k_2$. The bending energy U_b in the thin film is obtained by integrating the bending energy density W_b in Eq. (5) as

$$U_b = \frac{k_1}{2\pi}\frac{k_2}{2\pi}\int_{x_1=0}^{2\pi/k_1}\int_{x_2=0}^{2\pi/k_2} W_b dx_1 dx_2 = \frac{\bar{E}_f h_f^3}{96}(k_1^2+k_1^2)^2 A^2. \quad (12)$$

The shear stress at the film/substrate interface has a negligible effect on the wavelength and amplitude of the buckled film/substrate system.[12] The vanishing shear, together with Eq. (3), gives the governing equations for the in-plane displacement u_α, which have the solutions

$$u_1(x_1,x_2) = \frac{A^2[2k_1^2\cos^2(k_2x_2) - \nu_f k_2^2]}{16k_1}\sin(2k_1x_1),$$

$$u_2(x_1,x_2) = \frac{A^2[2k_2^2\cos^2(k_1x_1) - \nu_f k_1^2]}{16k_2}\sin(2k_2x_2). \quad (13)$$

Let $\varepsilon_{11}^0 = -\varepsilon_{11}^{\text{pre}}$ and $\varepsilon_{22}^0 = -\varepsilon_{22}^{\text{pre}}$, where $\varepsilon_{11}^{\text{pre}}$ and $\varepsilon_{22}^{\text{pre}}$ are the (positive) prestrains. The membrane energy U_m in the thin film is obtained by integrating the membrane energy density W_m in Eq. (6) as

$$\begin{aligned} U_m &= \frac{k_1}{2\pi}\frac{k_2}{2\pi}\int_{x_1=0}^{2\pi/k_1}\int_{x_2=0}^{2\pi/k_2} W_m dx_1 dx_2 \\ &= \frac{\bar{E}_f h_f}{256}[A^4(3-\nu_f^2)(k_1^4+k_2^4) + 4\nu_f A^4 k_1^2 k_2^2 \\ &\quad - 32A^2(k_1^2+\nu_f k_2^2)\varepsilon_{11}^{\text{pre}} - 32A^2(k_2^2+\nu_f k_1^2)\varepsilon_{22}^{\text{pre}} \\ &\quad + 128(\varepsilon_{11}^{\text{pre}})^2 + 128(\varepsilon_{22}^{\text{pre}})^2 + 256\nu_f\varepsilon_{11}^{\text{pre}}\varepsilon_{22}^{\text{pre}}]. \end{aligned} \quad (14)$$

The substrate is subjected to the normal displacement $w=A\cos(k_1x_1)\cos(k_2x_2)$ in Eq. (11) and vanishing shear traction on its top surface $(x_3=0)$, and vanishing shear and normal traction on its bottom surface $(x_3\to\infty)$. The displacements in the substrate are obtained analytically,

$$u_1(x_1,x_2,x_3) = \frac{(2\nu_s - 1 + \sqrt{k_1^2+k_2^2}x_3)k_1 A e^{-kx_3}}{2(1-\nu_s)\sqrt{k_1^2+k_2^2}} \times \sin(k_1x_1)\cos(k_2x_2),$$

$$u_2(x_1,x_2,x_3) = \frac{(2\nu_s - 1 + \sqrt{k_1^2+k_2^2}x_3)k_2 A e^{-kx_3}}{2(1-\nu_s)\sqrt{k_1^2+k_2^2}} \times \cos(k_1x_1)\sin(k_2x_2),$$

$$u_3(x_1,x_2,x_3) = \frac{(2-2\nu_s + \sqrt{k_1^2+k_2^2}x_3)A e^{-kx_3}}{2(1-\nu_s)} \times \cos(k_1x_1)\cos(k_2x_2), \quad (15)$$

where ν_s is the Poisson ratio of the substrate. The strain energy U_s in the substrate is obtained by integrating the strain energy density W_s in Eq. (10) as

Downloaded 03 Jan 2008 to 129.105.86.133. Redistribution subject to AIP license or copyright; see http://jap.aip.org/jap/copyright.jsp

$$U_s = \int_V W_s dV = \frac{k_1}{2\pi}\frac{k_2}{2\pi}\int_{x_1=0}^{2\pi/k_1}\int_{x_2=0}^{2\pi/k_2}\int_{x_3=0}^{\infty} W_s dx_1 dx_2 dx_3$$

$$= \frac{\bar{E}_s}{16}\sqrt{k_1^2+k_2^2}A^2, \tag{16}$$

where $\bar{E}_s$ is the plane-strain modulus of the substrate.

The minimization of the total energy U_{total}, which is the sum of film bending energy U_b in Eq. (12), the membrane energy U_m in Eq. (14), and the substrate strain energy U_s in Eq. (16), with respect to the amplitude A and wave numbers k_1 and k_2 gives

$$\frac{\partial U_{\text{total}}}{\partial A} = 2A\left\{\frac{\bar{E}_s}{16}\sqrt{k_1^2+k_2^2} + \frac{\bar{E}_f h_f^3}{96}(k_1^2+k_2^2)^2 + \frac{\bar{E}_f h_f}{128}[A^2(3-\nu_f^2)(k_1^4+k_2^4) + 4\nu_f A^2 k_1^2 k_2^2 - 16(k_1^2 + \nu_f k_2^2)\varepsilon_{11}^{\text{pre}} - 16(k_2^2+\nu_f k_1^2)\varepsilon_{22}^{\text{pre}}]\right\} = 0, \tag{17}$$

$$\frac{\partial U_{\text{total}}}{\partial k_1} = 2k_1A^2\left\{\frac{\bar{E}_s}{32}\frac{1}{\sqrt{k_1^2+k_2^2}} + \frac{\bar{E}_f h_f^3}{48}(k_1^2+k_2^2) + \frac{\bar{E}_f h_f}{128}[A^2(3-\nu_f^2)k_1^2 + 2\nu_f A^2 k_2^2 - 16\varepsilon_{11}^{\text{pre}} - 16\nu_f\varepsilon_{22}^{\text{pre}}]\right\} = 0, \tag{18}$$

$$\frac{\partial U_{\text{total}}}{\partial k_2} = 2k_2A^2\left\{\frac{\bar{E}_s}{32}\frac{1}{\sqrt{k_1^2+k_2^2}} + \frac{\bar{E}_f h_f^3}{48}(k_1^2+k_2^2) + \frac{\bar{E}_f h_f}{128}[A^2(3-\nu_f^2)k_2^2 + 2\nu_f A^2 k_1^2 - 16\nu_f\varepsilon_{11}^{\text{pre}} - 16\varepsilon_{22}^{\text{pre}}]\right\} = 0. \tag{19}$$

Equations (17)–(19) have the following analytical solutions:

$$k_1^2+k_2^2 = \frac{1}{h_f^2}\left(\frac{3\bar{E}_s}{\bar{E}_f}\right)^{2/3}, \tag{20}$$

$$k_1^2-k_2^2 = \frac{1}{h_f^2}\left(\frac{3\bar{E}_s}{\bar{E}_f}\right)^{2/3}\frac{3-\nu_f}{3+\nu_f} \times \frac{\varepsilon_{11}^{\text{pre}}-\varepsilon_{22}^{\text{pre}}}{\varepsilon_{11}^{\text{pre}}+\varepsilon_{22}^{\text{pre}}-[(3\bar{E}_s/\bar{E}_f)^{2/3}/2(1+\nu_f)]}, \tag{21}$$

$$A = 4h_f\left(\frac{\bar{E}_f}{3\bar{E}_s}\right)^{1/3}\sqrt{\frac{1}{3-\nu_f}\left[\varepsilon_{11}^{\text{pre}}+\varepsilon_{22}^{\text{pre}} - \frac{(3\bar{E}_s/\bar{E}_f)^{2/3}}{2(1+\nu_f)}\right]}. \tag{22}$$

For the equibiaxial prestrains $\varepsilon_{11}^{\text{pre}}=\varepsilon_{22}^{\text{pre}}=\varepsilon_{\text{pre}}$, Eq. (21) gives $k_1=k_2$, i.e., the checkerboard mode. The wave number and amplitude are obtained from Eqs. (20) and (22) as

$$k_1 = \frac{1}{\sqrt{2}}\frac{1}{h_f}\left(\frac{3\bar{E}_s}{\bar{E}_f}\right)^{1/3}, \tag{23}$$

$$A = h_f\sqrt{\frac{8}{(3-\nu_f)(1+\nu_f)}\left(\frac{\varepsilon_{\text{pre}}}{\varepsilon_{\text{checkerboard}}^c}-1\right)}, \tag{24}$$

where $\varepsilon_{\text{checkerboard}}^c=(3\bar{E}_s/\bar{E}_f)^{2/3}/4(1+\nu_f)$ is the critical strain for the checkerboard buckling mode.[9,10]

IV. HERRINGBONE BUCKLING MODE

The out-of-plane displacement w of the herringbone mode, as shown in Fig. 2(c), is periodic in both long wavelength direction x_2 and its perpendicular direction x_1 [also see Figs. 1(c) and 1(d)]. The contour line of constant w is sinusoidal in the x_1-x_2 plane [Figs. 1(c) and 1(d)], and therefore can be represented by $x_1+B\cos(k_2x_2)=\text{const}$, where B is the amplitude of the sinusoidal line, and $k_2=2\pi/\lambda_2$ is the corresponding wave number. The displacement of the herringbone mode is also sinusoidal in the x_1 direction (λ direction in Fig. 1), and therefore can be represented by[8]

$$w = A\cos\{k_1[x_1 + B\cos(k_2x_2)]\}, \tag{25}$$

where A is the amplitude and $k_1=2\pi/\lambda_1$ is the wave number, as shown in Figs. 1(c) and 1(d). Such a function is periodic in both x_1 and x_2 directions, and have the contour line $x_1+B\cos(k_2x_2)=\text{const}$. The bending energy U_b in the thin film is obtained by integrating the bending energy density W_b in Eq. (5) as

$$U_b = \frac{k_1}{2\pi}\frac{k_2}{2\pi}\int_{x_1=0}^{2\pi/k_1}\int_{x_2=0}^{2\pi/k_2} W_b dx_1 dx_2 = \frac{\bar{E}_f h_f^3}{384}k_1^2A^2(8k_1^2k_2^2B^2 + 4k_2^4B^2 + 3k_1^2k_2^4B^4 + 8k_1^2). \tag{26}$$

Similar to Sec. III, the vanishing shear at the film/substrate interface, together with Eq. (3), gives the governing equations for the in-plane displacements u_1 and u_2,

$$u_{1,11} + \frac{1}{2}(1-\nu_f)u_{1,22} + \frac{1}{2}(1+\nu_f)u_{2,12} + \frac{a_1(x_2)}{2}\sin(2k_1x_1) + \frac{b_1(x_2)}{2}\cos(2k_1x_1) - \frac{1}{4}(1-\nu_f)A^2k_1^2Bk_2^2 \times\cos(k_2x_2) = 0, \tag{27a}$$

$$u_{2,22} + \frac{1}{2}(1+\nu_f)u_{1,12} + \frac{1}{2}(1-\nu_f)u_{2,11} + \frac{a_2(x_2)}{2}\sin(2k_1x_1) + \frac{b_2(x_2)}{2}\cos(2k_1x_1) + \frac{1}{4}A^2k_1^2B^2k_2^3\sin(2k_2x_2) = 0, \tag{27b}$$

where $a_1(x_2)$, $b_1(x_2)$, $a_2(x_2)$, and $b_2(x_2)$ are the following

Downloaded 03 Jan 2008 to 129.105.86.133. Redistribution subject to AIP license or copyright; see http://jap.aip.org/jap/copyright.jsp

periodic functions of x_2, which can be expanded in Fourier series as

$$a_1(x_2) = A^2k_1^3\cos[2k_1B\cos(k_2x_2)][1+B^2k_2^2\sin^2(k_2x_2)] - \frac{1}{2}(1-\nu_f)A^2k_1^2Bk_2^2\cos(k_2x_2) \times \sin[2k_1B\cos(k_2x_2)] = \sum_{n=0}^{\infty} a_{1n}\cos(nk_2x_2), \tag{28a}$$

$$b_1(x_2) = A^2k_1^3\sin[2k_1B\cos(k_2x_2)][1+B^2k_2^2\sin^2(k_2x_2)] + \frac{1}{2}(1-\nu_f)A^2k_1^2Bk_2^2\cos(k_2x_2)\cos[2k_1B \times \cos(k_2x_2)] = \sum_{n=0}^{\infty} b_{1n}\cos(nk_2x_2), \tag{28b}$$

$$a_2(x_2) = -A^2k_1^3Bk_2\sin(k_2x_2)\cos[2k_1B\cos(k_2x_2)] \times [1+B^2k_2^2\sin^2(k_2x_2)] + \frac{1}{2}A^2k_1^2B^2k_2^3\sin(2k_2x_2) \times \sin[2k_1B\cos(k_2x_2)] = \sum_{n=1}^{\infty} a_{2n}\sin(nk_2x_2), \tag{28c}$$

$$b_2(x_2) = -A^2k_1^3Bk_2\sin(k_2x_2)\sin[2k_1B\cos(k_2x_2)] \times [1+B^2k_2^2\sin^2(k_2x_2)] - \frac{1}{2}A^2k_1^2B^2k_2^3\sin(2k_2x_2) \times \cos[2k_1B\cos(k_2x_2)] = \sum_{n=1}^{\infty} b_{2n}\sin(nk_2x_2). \tag{28d}$$

Here a_{1n}, b_{1n}, a_{2n}, and b_{2n} are the Fourier coefficients of $a_1(x_2)$, $b_1(x_2)$, $a_2(x_2)$, and $b_2(x_2)$, respectively. Equation (27) has the following analytical solutions:

$$u_1(x_1,x_2) = \sum_{n=0}^{\infty} f_{1n}\cos(nk_2x_2)\sin(2k_1x_1) + \sum_{n=0}^{\infty} g_{1n}\cos(nk_2x_2)\cos(2k_1x_1) - \frac{1}{2}A^2k_1^2B\cos(k_2x_2),$$

$$u_2(x_1,x_2) = \sum_{n=1}^{\infty} f_{2n}\sin(nk_2x_2)\sin(2k_1x_1) + \sum_{n=1}^{\infty} g_{2n}\sin(nk_2x_2)\cos(2k_1x_1) + \frac{1}{16}k_2A^2k_1^2B^2\sin(2k_2x_2), \tag{29}$$

where f_{1n}, g_{1n}, f_{2n}, and g_{2n} are

$$f_{1n} = \frac{-(1+\nu_f)nk_1k_2b_{2n} + 2(1-\nu_f)k_1^2a_{1n} + n^2k_2^2a_{1n}}{(1-\nu_f)(4k_1^2+n^2k_2^2)^2},$$

$$g_{1n} = \frac{(1+\nu_f)nk_1k_2a_{2n} + 2(1-\nu_f)k_1^2b_{1n} + n^2k_2^2b_{1n}}{(1-\nu_f)(4k_1^2+n^2k_2^2)^2},$$

$$f_{2n} = \frac{8k_1^2a_{2n} + 2(1+\nu_f)nk_1k_2b_{1n} + (1-\nu_f)n^2k_2^2a_{2n}}{2(1-\nu_f)(4k_1^2+n^2k_2^2)^2},$$

$$g_{2n} = \frac{8k_1^2b_{2n} - 2(1+\nu_f)nk_1k_2a_{1n} + (1-\nu_f)n^2k_2^2b_{2n}}{2(1-\nu_f)(4k_1^2+n^2k_2^2)^2}. \tag{30}$$

Let $\varepsilon_{11}^0 = -\varepsilon_{11}^{\text{pre}}$ and $\varepsilon_{22}^0 = -\varepsilon_{22}^{\text{pre}}$, where $\varepsilon_{11}^{\text{pre}}$ and $\varepsilon_{22}^{\text{pre}}$ are the (positive) prestrains. The membrane energy U_m in the thin film is obtained by integrating the membrane energy density W_m in Eq. (6) as

$$U_m = \frac{k_1}{2\pi}\frac{k_2}{2\pi}\int_{x_1=0}^{2\pi/k_1}\int_{x_2=0}^{2\pi/k_2} W_m dx_1dx_2 = \bar{E}_f h_f U_m^0(k_1A, k_2B, k_1B, \varepsilon_{11}^{\text{pre}}, \varepsilon_{22}^{\text{pre}}), \tag{31}$$

where U_m^0 is a nondimensional function that can be obtained analytically.

The substrate is subjected to, on its top surface ($x_3=0$), the vanishing shear traction and the normal displacement w in Eq. (25), which can be expanded in Fourier series as

$$w = \sum_{n=0}^{\infty}[A_{1n}\cos(k_1x_1)\cos(nk_2x_2) + B_{1n}\sin(k_1x_1)\cos(nk_2x_2)], \tag{32}$$

where A_{1n} and B_{1n} are the Fourier coefficients of $A\cos[k_1B\cos(k_2x_2)]$ and $-A\sin[k_1B\cos(k_2x_2)]$, respectively. The term $A_{10}\cos(k_1x_1)+B_{10}\sin(k_1x_1)$ for $n=0$ corresponds to the 1D buckling mode, while the terms for $n\geqslant 1$ correspond to the generalized checkerboard mode in the previous section. Using the linear superposition, we obtain the displacements in the substrate from the generalized checkerboard solution in Eq. (15) as

$$u_1(x_1,x_2,x_3) = \sum_{n=0}^{\infty}\frac{(2\nu_s - 1 + \sqrt{k_1^2+n^2k_2^2}x_3)k_1}{2(1-\nu_s)\sqrt{k_1^2+n^2k_2^2}} \times [A_{1n}\sin(k_1x_1) - B_{1n}\cos(k_1x_1)] \times \cos(nk_2x_2)e^{-\sqrt{k_1^2+n^2k_2^2}x_3},$$

Downloaded 03 Jan 2008 to 129.105.86.133. Redistribution subject to AIP license or copyright; see http://jap.aip.org/jap/copyright.jsp

$$u_2(x_1,x_2,x_3)=\sum_{n=0}^{\infty}\frac{(2\nu_s-1+\sqrt{k_1^2+n^2k_2^2}x_3)nk_2}{2(1-\nu_s)\sqrt{k_1^2+n^2k_2^2}}\times[A_{1n}\cos(k_1x_1)+B_{1n}\sin(k_1x_1)]\times\sin(nk_2x_2)e^{-\sqrt{k_1^2+n^2k_2^2}x_3},$$

$$u_3(x_1,x_2,x_3)=\sum_{n=0}^{\infty}\frac{2-2\nu_s+\sqrt{k_1^2+n^2k_2^2}x_3}{2(1-\nu_s)}[A_{1n}\cos(k_1x_1)+B_{1n}\sin(k_1x_1)]\cos(nk_2x_2)e^{-\sqrt{k_1^2+n^2k_2^2}x_3}. \quad (33)$$

The strain energy U_s in the substrate is obtained by integrating the strain energy density W_s in Eq. (10) as

$$U_s=\frac{\bar{E}_s}{16}\sum_{n=1}^{\infty}\sqrt{k_1^2+n^2k_2^2}(A_{1n}^2+B_{1n}^2)+\frac{\bar{E}_s}{8}k_1(A_{10}^2+B_{10}^2)=\bar{E}_sk_1A^2U_s^0(k_1B), \quad (34)$$

where U_s^0 is a nondimensional function of k_1B that can be obtained analytically.

The total energy is the sum of the film bending energy U_b in Eq. (26), the membrane energy U_m in Eq. (31), and the substrate strain energy U_s in Eq. (34). The minimization of U_{total} with respect to A, B, k_1, and k_2 gives their governing equations, which are solved by the quasi-Newton and finite difference gradient method given in the IMSL program.[18] For each given k_2, there are multiple local minima for the large range of initial values of A (from 0 to 10 μm), B (from 0 to 100 μm), and k_1 (from 0 to 10 μm^{-1}). The global minimum (with respect to A, B, and k_1) is obtained by comparing all local minima in the range.

V. ONE-DIMENSIONAL BUCKLING MODE

The 1D buckling mode $w=A\cos(k_1x_1)$ shown in Fig. 2(a) is the special case of the herringbone buckling mode in Eq. (25) with $B=0$. For the 1D mode the film bending energy, the membrane energy, and the substrate strain energy are obtained analytically as

$$U_b=\frac{\bar{E}_fh_f^3}{48}k_1^4A^2, \quad (35)$$

$$U_m=\frac{\bar{E}_fh_f}{2}\left[\left(\frac{1}{4}k_1^2A^2-\varepsilon_{11}^{\text{pre}}\right)^2+(\varepsilon_{22}^{\text{pre}})^2-2\nu_f\left(\frac{1}{4}k_1^2A^2-\varepsilon_{11}^{\text{pre}}\right)\varepsilon_{22}^{\text{pre}}\right], \quad (36)$$

$$U_s=\frac{\bar{E}_s}{8}k_1A^2. \quad (37)$$

The minimization of total energy U_{total} with respect to A and k_1 gives their analytical solutions,

$$k_1=\frac{1}{h_f}\left(\frac{3\bar{E}_s}{\bar{E}_f}\right)^{1/3}, \quad (38)$$

$$A=h_f\sqrt{\frac{\varepsilon_{11}^{\text{pre}}+\nu_f\varepsilon_{22}^{\text{pre}}}{(1/4)(3\bar{E}_s/\bar{E}_f)^{2/3}}-1}. \quad (39)$$

The wave number k_1 (and therefore the wavelength $\lambda_1=2\pi/k_1$) does not depend on the prestrain, but the amplitude A does. For plane-strain buckling $\varepsilon_{22}^{\text{pre}}=0$, the wavelength and amplitude are the same as those given by prior 1D buckling models.[5,9,10,12] For equibiaxial prestrains $\varepsilon_{11}^{\text{pre}}=\varepsilon_{22}^{\text{pre}}=\varepsilon_{\text{pre}}$, the amplitude becomes

$$A=h_f\sqrt{\frac{\varepsilon_{\text{pre}}}{\varepsilon_{1\text{D}}^c}-1}, \quad (40)$$

where $\varepsilon_{1\text{D}}^c=(3\bar{E}_s/\bar{E}_f)^{2/3}/4(1+\nu_f)$ is the critical strain for the 1D buckling mode, and is the same as that for the checkerboard buckling mode given near the end of Sec. III.

It is important to point out that the 1D mode cannot be obtained from the generalized checkerboard mode in Sec. III. Even though the displacement in Eq. (11) degenerates to the 1D buckling mode when $k_2=0$, the bending energy in Eq. (12) does not, and is different from its counterpart for 1D buckling mode by a factor of 2. This is because the bending energy in Eq. (12) involves the average $k_1/2\pi k_2/2\pi\int_0^{2\pi/k_1}\int_0^{2\pi/k_2}\cos^2(k_1x_1)\cos^2(k_2x_2)dx_1dx_2$, which equals $1/4$ for $k_2\neq0$ (generalized checkerboard mode) but equals $1/2$ for $k_2=0$ (1D mode).

VI. RESULTS AND DISCUSSION

The three different buckling modes (1D, checkerboard, and herringbone) are studied for the Si film/PDMS substrate. The mechanical properties of Si (Ref. 19) and PDMS (Ref. 20) are $E_f=130$ GPa, $E_s=1.8$ MPa, $\upsilon_f=0.27$, and $\upsilon_s=0.48$. The critical buckling strain is 0.0267% for the 1D and checkerboard modes, and the numerical results give the same (0.0267%) for the herringbone mode. The prestrain is introduced by thermal expansion, which gives equibiaxial compression ($\varepsilon_{11}^{\text{pre}}=\varepsilon_{22}^{\text{pre}}=\varepsilon_{\text{pre}}$) in Si. The 1D and checkerboard modes have analytical solutions, but only numerical results are obtained for herringbone mode.

For the 100 nm thick Si thin film, the wavelengths $\lambda_1=2\pi/k_1$ are 24.11 μm from Eq. (23) for the checkerboard mode, and 17.05 μm from Eq. (38) for the 1D mode. The total energy for the herringbone mode has minimum with respect to the amplitude of the herringbone A, wave number k_1, and amplitude of jogs B for each given long wavelength $\lambda_2=2\pi/k_2$, but it has no minimum with respect to λ_2. Figure 5 shows the ratio of total energy U_{total} in the buckled state to that in the unbuckled state $U_0=\bar{E}_fh_f(1+\nu_f)\varepsilon_{\text{pre}}^2$ versus the long wavelength λ_2 for herringbone mode under 2.4% prestrain. The curve clearly does not have a minimum, and becomes essentially a constant for λ_2 exceeding 110 μm. This lack of energy minimum with respect to the long wavelength has also been observed in the finite element analysis.[10] It is also consistent with the experimental results[8] shown in Fig. 4, which gives a wide range of long wavelengths in a domain subjected to the same prestrain.

Figure 6(a) shows the amplitude of jogs B versus the long wavelength λ_2 for three different prestrains, 0.5%,

Downloaded 03 Jan 2008 to 129.105.86.133. Redistribution subject to AIP license or copyright; see http://jap.aip.org/jap/copyright.jsp

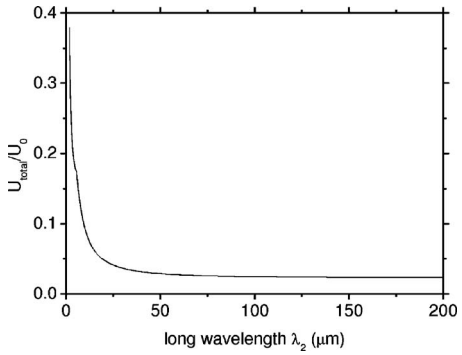

FIG. 5. Ratio of total energy in the buckled state to its counterpart in the unbuckled state U_{total}/U_0 vs the long wavelength λ_2 for herringbone mode under 2.4% prestrain. The film thickness is 100 nm.

1.5%, and 2.4%. B is not only linearly proportional to λ_2, it is also independent of the prestrain since all three straight lines coincide. This suggests that the contour line of the herringbone, $x_1+B\cos(2\pi x_2/\lambda_2)=\text{const}$, remains self-similar for different λ_2 and prestrain. Figure 6(b) shows the jog angle $\theta=\pi-2\tan^{-1}(k_2B\pi/4)$ versus the long wavelength λ_2, where θ is obtained by using $B\cos(k_2x_2)$ as the first term of the Fourier series of the zigzag function. Except for λ_2 less than 20 μm, the jog angle is essentially a constant close to 90°, and is independent of the prestrain. This once again confirms the self-similarity of the herringbone contour. Figures 6(c) and 6(d) show the short wavelength λ and amplitude of herringbone A versus the long wavelength λ_2, respectively, where $\lambda=2\pi/[k_1\sqrt{1+(k_2B\pi/4)^2}]$ is also obtained by using $B\cos(k_2x_2)$ as the first term of the Fourier series of the zigzag function. For large λ_2, both λ and A have asymptotes. The asymptote for λ is independent of the prestrain, but that for A depends on the prestrain. These prestrain-independent wavelength and prestrain-dependent amplitude are consistent with the prior model for 1D buckling at small prestrain.[5,12,18] The above observations in Fig. 6 also agree with the prior finite element analysis.[9,10]

The short wavelength λ measured in experiments[8] is about 13.0 μm at the prestrain 2.4%, which is much smaller than that of 1D buckling mode. For this λ and $\varepsilon_{\text{pre}}=2.4\%$, the long wavelength $\lambda_2=2\pi/k_2$ obtained from Fig. 6(c) is about 40 μm, and the corresponding amplitude of jog B obtained from Fig. 6(a) is about 9 μm. These values all fall into the range reported in the experiments.[8]

As seen from Fig. 5, the energy of herringbone mode becomes unchanged with the long wavelength λ_2 for λ_2 larger than 110 μm. Figure 7(a) shows the ratio of the total energy U_{total} (for λ_2 larger than 110 μm) to U_0 versus the prestrain for three different buckling modes: 1D, checkerboard, and herringbone. The herringbone mode gives the lowest energy, and is therefore energetically favorable mode in 2D buckling. Figures 7(b)–7(d) provide an explanation by giving the ratios of substrate strain energy U_s, thin film bending energy U_b, and membrane energy U_m to U_0. The film membrane energy of the herringbone mode is much lower than other two modes [see Fig. 7(d)] although its substrate strain energy and film bending energy are slightly higher than their counterparts [Figs. 7(b) and 7(c)]. The herringbone mode significantly reduces the thin film membrane energy at the expense of slight increase of the thin film bending energy and substrate strain energy. This conclusion holds for the buckling of stiff thin film/compliant substrate system at all strain levels.

The above observation of herringbone being the ener-

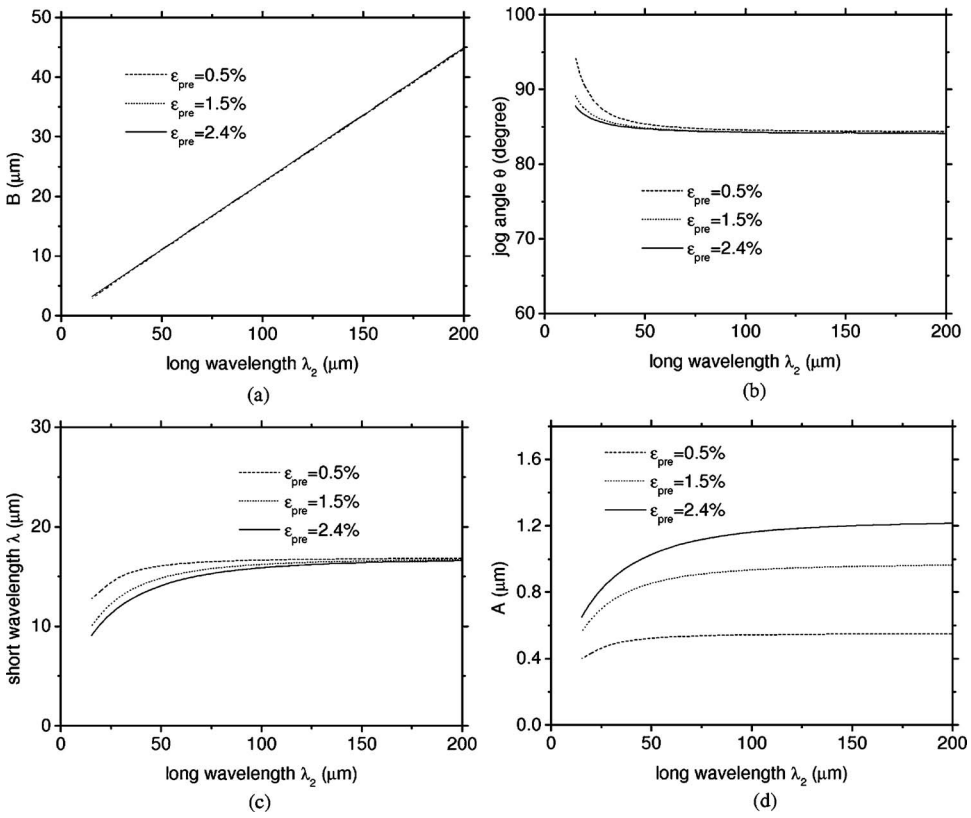

FIG. 6. (a) Amplitude of jogs B, (b) jog angle θ, (c) short wavelength λ, and (d) amplitude A vs long wavelength λ_2 for herringbone mode under 0.5%, 1.5%, and 2.4% prestrains. The film thickness is 100 nm.

Downloaded 03 Jan 2008 to 129.105.86.133. Redistribution subject to AIP license or copyright; see http://jap.aip.org/jap/copyright.jsp

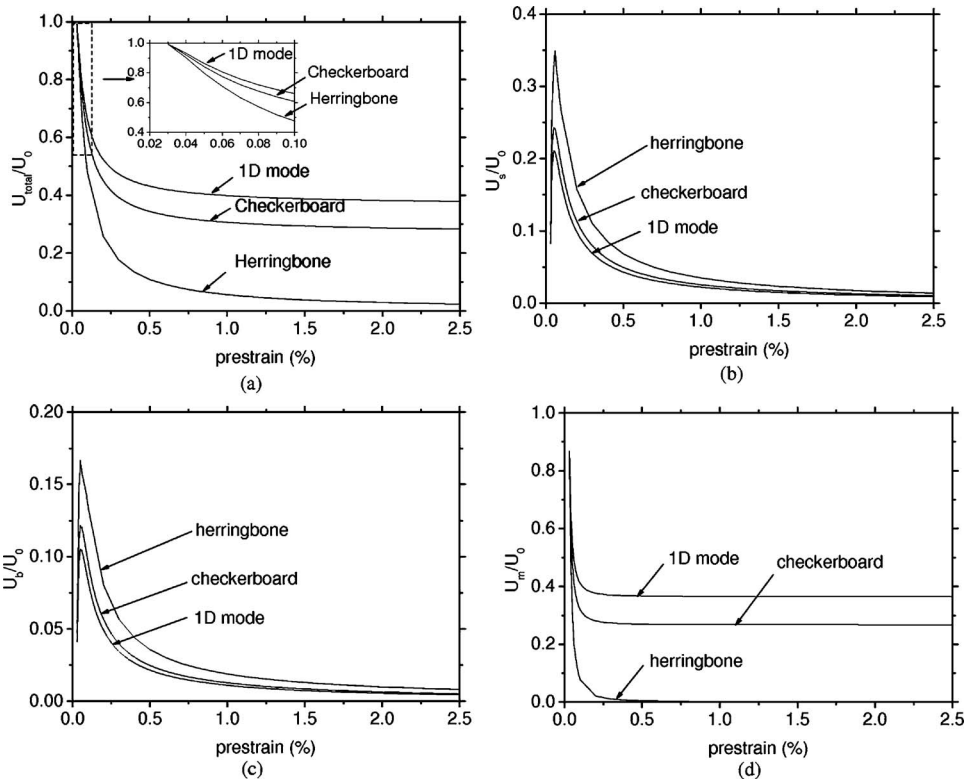

FIG. 7. Ratios of energy in the buckled state to that in the unbuckled state U_0 vs the prestrain ε_{pre} for 1D, checkerboard, and herringbone modes; (a) Total energy U_{total} in the Si film/PDMS substrate system; (b) strain energy U_s, in the PDMS substrate; (c) bending energy U_b in the Si film; and (d) membrane energy U_m in the Si film.

getically favorable buckling mode, however, holds for the equibiaxial prestrain. For other strains, herringbone may not always be the favorable mode. For example, the 1D mode predominates at the free edges, while 2D herringbone mode is typically observed in the inner region.[8] This is because the stress (or strain) state changes from the equibiaxial in the inner region to 1D near the free edge.

Strictly speaking Si is not elastically isotropic but has cubic symmetry. The material properties of anisotropy Si are $C_{11}=165.7$ GPa, $C_{12}=63.9$ GPa, and $C_{44}=79.6$ GPa. We have calculated the amplitude A and short wavelength λ_1 for the Si thin film with cubic symmetry. They are all within 5% of their elastically isotropic counterparts, under 2.4% prestrain, i.e., the cubic symmetry has little effect on the amplitude and short wavelength.

VII. CONCLUDING REMARKS

We have established an analytic approach to study the 1D, checkerboard, and herringbone buckling patterns in a stiff thin film on a compliant substrate system. The herringbone mode energy gives the lowest energy for the film/substrate system subjected to equibiaxial prestrain, which explains why herringbone mode is frequently observed in experiments with thermally induced prestrain. As compared to the 1D or checkerboard modes, the herringbone mode significantly reduces the thin film membrane energy at the expense of slight increase of the thin film bending energy and substrate strain energy. The 1D mode, however, may appear near the thin film free edge.

ACKNOWLEDGMENTS

We acknowledge the support from the National Science Foundation under Grant No. DMI-0328162, and the U.S. Department of Energy, Division of Materials Sciences under Award No. DEFG02-91ER45439, through the Frederick Seitz MRL and Center for Microanalysis of Materials at the University of Illinois at Urbana-Champaign. H.J. acknowledges the support from NSF No. CMMI-0700440, and Y.H. acknowledges the support from NSFC.

[1] H. C. Jin, J. R. Abelson, M. K. Erhardt, and R. G. Nuzzo, J. Vac. Sci. Technol. B **22**, 2548 (2004).
[2] V. Lumelsky, M. S. Shur, and S. Wagner, IEEE Sens. J. **1**, 41 (2001).
[3] T. Someya, T. Sekitani, S. Iba, Y. Kato, H. Kawaguchi, and T. Sakurai, Proc. Natl. Acad. Sci. U.S.A. **101**, 9966 (2004).
[4] A. Nathan, B. Park, A. Sazonov, S. Tao, I. Chan, P. Servati, K. Karim, T. Charania, D. Striakhilev, Q. Ma, and R. V. R. Murthy, Microelectron. J. **31**, 883 (2000).
[5] D. Y. Khang, H. Jiang, Y. Huang, and J. A. Rogers, Science **311**, 208 (2006).
[6] Y. Sun, V. Kumar, I. Adesida, and J. A. Rogers, Adv. Mater. (Weinheim, Ger.) **18**, 2857 (2006).
[7] Y. Sun, W. M. Choi, H. Jiang, Y. Huang, and J. A. Rogers, Nat. Nanotechnol. **1**, 201 (2006).
[8] W. M. Choi, J. Song, D. Y. Khang, H. Jiang, Y. Huang, and J. A. Rogers, Nano Lett. **7**, 1655 (2007).
[9] X. Chen and J. W. Hutchinson, Scr. Mater. **50**, 797 (2004).
[10] X. Chen and J. W. Hutchinson, J. Appl. Mech. **71**, 597 (2004).
[11] Z. Y. Huang, W. Hong, and Z. Suo, Phys. Rev. E **70**, 030601 (2004).
[12] Z. Y. Huang, W. Hong, and Z. Suo, J. Mech. Phys. Solids **53**, 2101 (2005).
[13] R. Huang and Z. Suo, J. Appl. Phys. **91**, 1135 (2002).
[14] R. L. Peterson, K. D. Hobart, F. J. Kub, H. Yin, and J. C. Sturm, Appl. Phys. Lett. **88**, 201913 (2006).
[15] R. Huang and H. S. Im, Phys. Rev. E **74**, 026214 (2006).

Downloaded 03 Jan 2008 to 129.105.86.133. Redistribution subject to AIP license or copyright; see http://jap.aip.org/jap/copyright.jsp

[16]S. Timoshenko, *Theory of Plates and Shells* (McGraw-Hill, New York, 1940).
[17]S. Timoshenko and J. N. Goodier, Theory of Elasticity, 3rd ed. (McGraw-Hill, New York, 1969).
[18]IMSL FORTRAN 90 MP Library, Compaq Visual FORTRAN 6.0.
[19]*Properties of Silicon* (INSPEC/Institution of Electrical Engineers, New York, 1998).
[20]A. Bietsch and B. Michel, J. Appl. Phys. **88**, 4310 (2000).

Downloaded 03 Jan 2008 to 129.105.86.133. Redistribution subject to AIP license or copyright; see http://jap.aip.org/jap/copyright.jsp